Heat and Mass Transfer
https://doi.org/10.1007/s00231-021-03127-5

ORIGINAL

Thermal management system based on closed-loop pulsating heat pipe for electric motors

Mithun Sundar S[1] · Swathi S[1] · Kailash S. Prem[1] · Chithrakumar V. K[1]

Received: 1 March 2021 / Accepted: 25 August 2021

Abstract

Thermal management of electric motor is a significant criterion concerning the performance of the motor since it relies on the working temperature. This paper presents an experimental investigation of a thermal management system with a design based on the passive action of closed-loop pulsating heat pipes (CLPHP). The evaporator is a curved copper section termed the cooling pad, which inculcates the pulsating fluid regime and directly contacts the motor surface. Four such sets of CLPHPs are mounted on a test bench to study the performance characteristics of the system. Water–acetone binary mixture is selected as the working fluid and is tested for optimum mixing ratio by varying the acetone concentration through 40%, 50% and 60%. Performance study is carried out under different current readings of 1 A, 2 A, and 3 A, resulting in respective heat loads of 27 W, 109 W, and 240 W until the steady-state temperature is achieved. Filling ratios (FR) are taken as 40%, 50% and 60% of the total volume. The results obtained show that a 50% filling ratio with a 50% mixing ratio (MR) gives the optimum working condition by which the cooling system can reduce the motor temperature by 33.3 °C with a 47% increase in overall heat transfer coefficient compared to the natural convection of motor surface.

Nomenclature

A	Area (m^2)
Bo	Bond number
D	Diameter (m)
Eö	Eötvös number = $(Bo)^2$
Q	Heat input (W)
R	Thermal resistance (K/W)
T	Temperature (˚C)
ΔT	$T_e - T_\infty$ (˚C)
U	Coefficient of overall heat transfer (W/m^2-K)
V	Voltage (V)
I	Current (A)
U_{max}	Maximum uncertainty
σ	Surface tension (N/m)
ρ	Density (Kg/m^3)
a	Ambient
crit	Critical
e	Evaporator
liq	Liquid
vap	Vapour

1 Introduction

Heat dissipation in electric motors has always been a subject of interest for many researchers, continuously trying and bringing new design developments to reduce the thermal loads and increase the efficiency of the motor. The main sources of heat generation in a motor are the I^2R losses, the core loss, the stray load loss, and the bearing system losses. Among them the major loss is considered to be the stator resistance loss. This undesirable heat generation causes a spike in stator coil temperatures and often leads to problems such as increased stator winding deterioration, reduced motor performance and power limitation as well as reduces the overall life expectancy of the motor. Furthermore, a higher temperature can lead to the demagnetization of the permanent magnet in electric motors. Thus, it is essential to incorporate a cooling system in an electric motor since lowering the excessive temperature in the stator will translate to higher motor performances and efficiencies along with longer life expectancy of the motor [1–3].

Over the years several studies on cooling systems have been introduced to tackle this problem. However, the most common method used for motor cooling has fins mounted on its external surface to increase the heat dissipation which may be aided by an external or internal fan or simply by the free convection of air. Another alternative is a liquid cooling

✉ Chithrakumar V. K
chithrakumar@sctce.ac.in

[1] Department of Mechanical Engineering, Sree Chithra Thirunal College of Engineering, 695018 Trivandrum, India

Published online: 18 September 2021

system which can be provided in a multitude of ways. One of them is to circulate a 'coolant' through pipes on the outer body of the motor and another one is spiral flow across the outer periphery of the motor. Mohamed Amine et al. [4] studied thermal analysis of an electric vehicle motor based on the heat sources and geometry of the vehicle. The temperature at different parts of an electric motor is noted and two systems of water-cooling and air-cooling were developed and analyzed. It has been shown that water cooling is more efficient compared to air cooling since the specific heat of water is 4217 J/Kg°C while air is 1060 J/Kg°C. Although most of the experimental researches reviewed were about active cooling devices, the purpose of this work is to design and test a passive method that provides significant results.

Heat pipes are one of the emerging and promising technologies in the field of cooling applications for many electrical components since it is a passive heat transfer device having advantages over other cooling techniques such as being low cost, energy-efficient, and reliable operation [5, 6]. Groll et al. [7] incorporated heat pipes on to the stator and rotor for developing a more efficient cooling system than that of a conventional one. It was found that a maximum temperature of 150 °C is attained in the stator section. Heat dissipated in the rotor and stator attributed to almost 75% of the heat dissipated to the air through convection. Putra et al. [8] developed an electric motor design for better heat dissipation by providing L-shaped wicked flat heat pipes on the outer surface of the motor. The result obtained shows a significant reduction in temperature.

The pulsating heat pipe (PHP) proposed by Akachi [9] in 1990 found to be best suited for cooling purpose. The features of pulsating heat pipe such as high heat flux transfer, passive working, fewer mechanical parts and absence of a wick structure make it an attractive alternative. A Pulsating Heat Pipe based cooling system, when compared with a liquid cooling system, is less complex due to its more compact nature. Khandekar et al. [10] summarized the basic construction details, the various parameters which influence the heat transfer mechanism such as (i) Tube diameter (ii) Applied heat flux, (iii) Working fluid ratio, (iv) Total number of turns, and (v) Operating orientation. Yang et al. [11] to understand the operating limit of Closed-loop Pulsating Heat Pipe (CLPHP) studied the effects of (i) Operating orientation (ii) Inner diameter and (iii) Filling ratio. The effect of the three different heat modes; (a) bottom heat mode (b) horizontal heat mode (c) top heat mode, on the performance of heat pipes using working fluid R142b has shown that on decreasing inner diameter from 2 to 1 mm, the effect of orientation becomes negligible. It has been found that CLPHPs with 1 mm or 2 mm diameter operates successfully under three orientations with good performance. Also, a lower thermal resistance of about 10% is shown by 2 mm ID compared with 1 mm ID. The best performance for all types of orientation was found to be the one with a filling ratio of 50%.

Vipul M. Patel et al. [12] conducted experiments on different types of working fluids used in cooling operations and studied the startup mechanism and thermal performance of a closed-loop pulsating heat pipe. Based on the results, it was found that among pure fluids, acetone shows the best heat transfer performance and among binary fluids, water–acetone gives better performance. Mozumder et al. [13] developed and fabricated a heat pipe and tested for performance against common working fluids including water, methanol, and acetone. The overall heat transfer coefficient for methanol and acetone filled heat-pipe shows an increase with the increase in heat input while water-filled heat pipe is nearly constant. Wilson et al. [14] conducted a thermal and visual observation of oscillating heat pipes (CLPHP) having working fluid water and acetone and came up with some general conclusions that acetone-based CLPHP shows a higher fluid velocity, full circulation, and better thermal performance over water-filled CLPHP. Also, it was observed that acetone CLPHP can produce higher temperature uniformity at low heat input. Better thermal performance is shown by acetone at lower temperatures and by water at higher temperatures.

In this study, working fluid is the binary mixture of water and acetone since it has lower specific heat and latent heat, which helps in creating strong pressure impulses for driving the working fluid and hence facilitates more heat flux transferred for the same thermal capacity. It is observed that in comparison with pure water, the water–acetone mixture exhibited better start-up performance due to its lower boiling point and low specific heat capacity. Also, the water–acetone mixture shows improved performance against 'dry-out' condition under low filling ratios of 35% and 45%. This is because at higher temperatures acetone vapours will be more and water will remain largely in the liquid phase which prevents the onset of dry out [15].

For the past 10 years, many experiments and investigations were conducted on developing pulsating heat pipes and enhancing their performance parameters. Furthermore, several research works were carried to find out the operating characteristics of pulsating heat pipes under a wide range of working fluids. The literature study conducted in the fields of pulsating heat pipes reveals that so far most of the works have been performed in the interest of analysis of thermal performances and increasing the efficiency of the heat pipes. Only fewer studies addressed CLPHP as a potential cooling system in electric motors. Also, the application of binary mixtures as working fluids in heat pipes is a briefly touched topic in regards to cooling systems. In this work, a passive heat transfer cooling method based on the working principle of a CLPHP is designed for electric motors and is experimentally analysed. Water–acetone binary solution is

taken as the working fluid and experiments were conducted in heat inputs 27 W, 109 W and 240 W for various mixing ratios (MR) and filling ratios (FR) to find out the optimum combination which yields the best performance for the given cooling system.

2 Methodology

2.1 Construction

The state of the art on the comprehensive theory of the intricate thermo-hydrodynamic phenomenon governing the proper functioning of a closed-loop pulsating heat pipe is still under research and not readily available [16]. But progressive research on this topic for the past decade validated many qualitative and quantitative parameters influencing the thermal performance of this technology.

The foremost parameter amongst other key factors considered for the fabrication of a closed-loop pulsating heat pipe is the inner diameter. Akachi et al. [9] primarily proposed that the critical Bond number (or Eötvös) criterion ensures the maximum tolerable inner diameter of any pulsating heat pipe based on the working fluid properties:

$$(\text{Eö})_{crit} = (\text{Bo})^2_{crit} \approx \frac{D^2_{crit} \cdot g \cdot (\rho_{liq} - \rho_{vap})}{\sigma} \approx 4 \quad (1)$$

In this experiment, the diameter of the capillary tube is selected as 2 mm from the lowest critical range of diameter according to the critical diameter for different pure fluids under different temperatures [17], which is below the Eö = 4 range since at Eö > 4 pulsating action diminishes and surface tension reduces [10]. Also based on the literature study on working fluid used in closed-loop pulsating heat pipes suggests that the selected inner diameter ensures the proper pulsation phenomena without any agglomeration and stratification of phases of the working fluid.

Figures 1, 2 displays the design of the closed-loop pulsating heat pipe-based cooling system used in this experiment. Beryllium copper was used for the fabrication of the evaporator section (cooling pad) and pure industrial grade copper tubes of 2 mm inner diameter and 3 mm outer diameter was used for the heat pipes. For the fabrication of the evaporator section, copper blocks were CNC machined to form curved planar sections having an inner radius of 90 mm, length of 100 mm and thickness of 8 mm. Cooling pad sections were micro-machined with eight through-holes to contain the pulsating action advancing from the condenser region. Copper tubes were cut and bent into the required length and bending radius, then fixed each pipe section coaxial to the holes in the cooling pads and hermetically sealed all tube sections by brazing with copper-based solder alloy ensuring proper

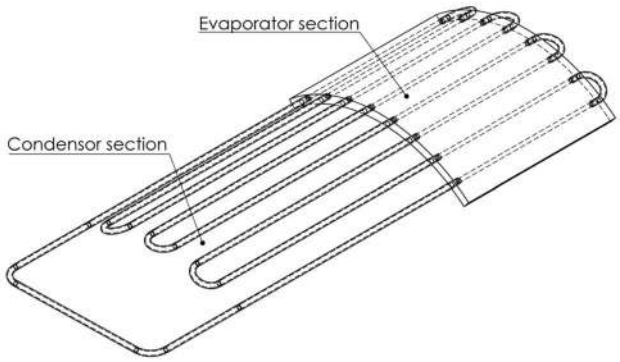

Fig. 1 Closed-loop pulsating heat pipe embedded with cooling pad

thermal contact. Valves were also attached for the charging and evacuation purposes of the CLPHP.

Length of condenser section = 150 mm + 60 mm
Length of evaporator section = 100 mm.
No of condenser section pipe turns (on each pad) = 150 mm length × 3
210 mm valves attached turn x 1
U-turns (bending radius 15 mm) x 4pcs.
Thickness of cooling pad = 8 mm
Arc radius of cooling pad = 90 mm (inner), 98 mm (outer).

This procedure is repeated to fabricate four individual CLPHPs as shown in Fig. 3 for the proposed experiment. An aluminium block was machined into a hollow cylinder with 100 mm length and 4 mm thickness. Ni–Cr thermic wire of diameter 12 mm is coiled in a helical fashion (180 mm dia.) and placed in contact with the inner surface of the cylinder. Thus by adjusting the current in the heating coil, the real-time heat load in a motor surface can be simulated and is used throughout this experiment.

2.2 Configuration

The literature survey conducted on various motor cooling methods and motor characteristics including that of a permanent magnet synchronous motor (PMSM) reveal

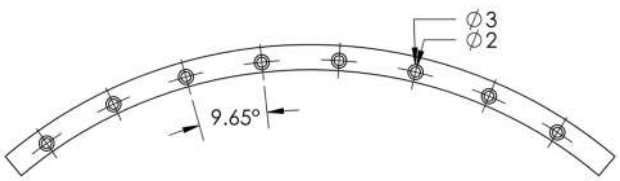

Fig. 2 Cross-sectional view of cooling pad (hole configuration)

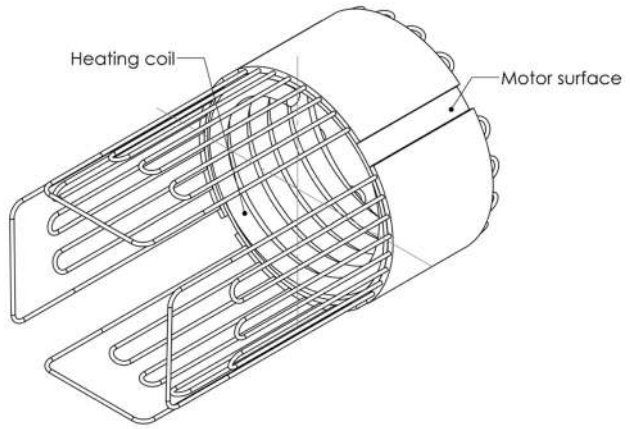

Fig. 3 Assembled model of CLPHP

that a comprehensive thermal management system of an electric motor attempts to attain the maximum possible torque without compromising the health of the permanent magnet and the copper winding. The rate of heat transfer in these motors can range between a few hundred watts to kilowatts depending on the motor class, RPM and loading [18–20]. The maximum allowable winding temperature in class F and class H motor insulations are 155 °C and 180 °C respectively [21]. Any increase in temperature above these limits will reduce the service life of the insulation and the overall life expectancy of the motor. A higher motor temperature will incite demagnetization of the permanent magnet which will then directly affect the motor efficiency [22].

Khandekar et al. [10] summarized the influencing parameters on the complex thermo-hydrodynamic of pulsating heat pipes and as per the findings, the effect of applied heat flux at higher temperatures will lead to the onset of dry-out induced by the thermo-hydrodynamic limitation. An experimental investigation on the start-up heat and other thermal attributes of CLPHP under water–acetone with different filling ratios was conducted by Zhu et al. [15], which acknowledges the dry-out condition of pulsating heat pipe at higher heat fluxes. In this work, the thermal configuration is made in such a way that the proposed CLPHP system will undergo a passive operation in still air without any forced convective assistance at the condenser section. The whole CLPHP arrangement is installed on a cylindrical heat source which is used to simulate real motor surface temperature variations. Taking the dry-out condition of the water–acetone binary mixture and the maximum allowable winding temperature of class F motors into consideration, the maximum operating temperature is restricted to 130 °C. Heat loads of 27 W, 109 W and 240 W were applied by stepping up each ampere of current (1 A, 2 A and 3 A) through the heating coil. At 240 W, the maximum permitted limit of 130 °C has reached and selected as the highest heat load to be tested.

Table 1 Details of working fluid combinations

Mixing Ratio (MR) (%)		Filling Ratio (FR) (%)
Acetone	Water	
50	50	40
50	50	50
50	50	60
40	60	50
60	40	50

The motor/heat-generating surface is thermo-physically covered with the evaporator regions so that the CLPHP can gain maximum heat flux. Sameer Khandekar et al. suggests the increased number of turns ultimately suppress the heat transferred by each turn [10], therefore, the turns of heat pipes were split and accommodated into four individual CLPHPs to allow improved heat transfer without affecting the circulation pressure drops. Figure (3) depicts the assembled configuration of closed-loop pulsating heat pipes over the motor/heat-generating surface. A thermally conductive paste was used to decrease the thermal resistance at the contact surfaces while mounting each evaporator section (cooling pad).

Ten J-type thermocouple wires of 0.3 mm diameter with an accuracy of ±0.1°C were used to measure the temperature readings. Thermocouples were paired in two sets of five and each set was mounted diametrically opposite to the cylinder.

2.3 Experimental procedure

Since the pulsating heat pipes constructed for this experiment involves few brazed joints all around evaporator sections and valves, a standard industrial leak test which includes immersed gas bubble visual inspection, compressed N_2 (130 psi) charged snoop test, and helium leak test were conducted and found to be successful. The CLPHPs were chemically cleaned to remove oxidative coatings and baked to 130 °C to evacuate any residual vapour contents trapped inside the copper tubes. A vacuum pressure of 0.01 mbar is maintained inside the CLPHP by using a turbopump (Pfeiffer-HiCube 700 Pro) working in serial action with a vane pump. The water–acetone binary mixtures are precisely prepared (as listed in Table 1).

The schematic of the experimental setup is shown in Fig. 4 and it consists of a power supply unit, the CLPHP unit and a data acquisition system to read temperature variations. An autotransformer, ammeter and a voltmeter connected to the heating coil execute the power supply unit. The heating coils were connected to the autotransformer to supply the required power. A data acquisition

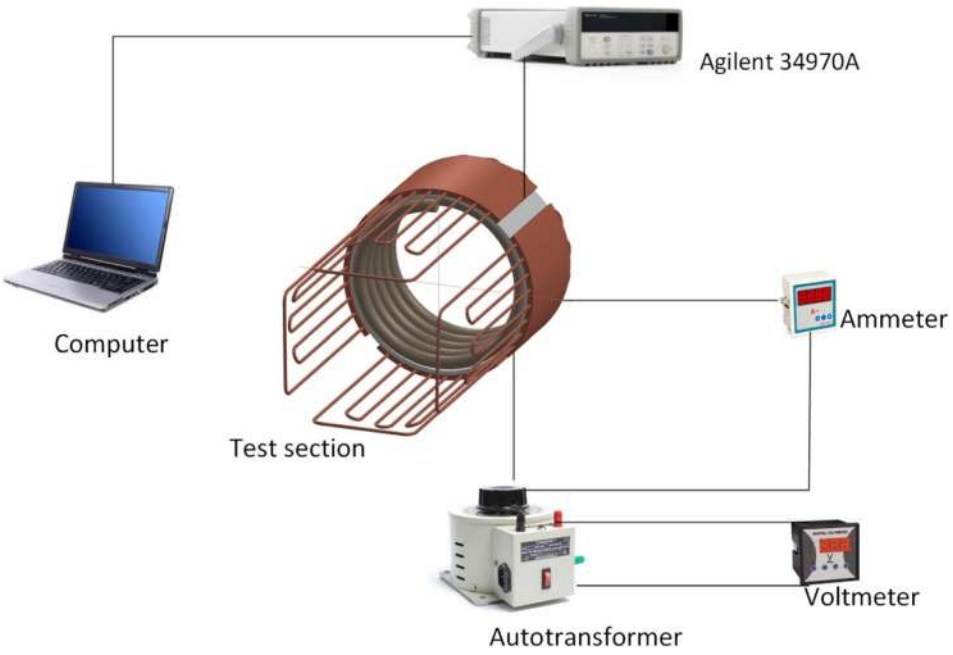

Fig. 4 Schematic of experimental Setup

system (Agilent 34970A) with 20 channel multiplexer (Agilent 34901A) connected to thermocouples was used to read and record data into the computer.

The entire assembly is installed on a test bench and maintained in a horizontal orientation. The dissipation of heat from the condenser section takes natural convection to the atmosphere (still air). Experiments were conducted to observe the thermal characteristics of our thermal management system from ambient temperature to steady-state condition. For each test run, the system has been brought back to ambient temperature to understand the fluid performance under different combinations. As mentioned before, the water–acetone binary mixture is taken as the working fluid for CLPHPs and is investigated for performance characteristics under different MR and FR. Combinations of MR and FR of the water–acetone mixture chosen in this experiment are listed in Table 1. In addition to that, a test run of the heating surface without employing CLPHPs was also done as reference data to compare with other test results for the performance evaluation. Observations are carried under different current readings of 1 A, 2 A, and 3 A, resulting in respective heat loads of 27 W, 109 W, and 240 W until the steady-state temperature is achieved. To find out the optimum FR for the thermal management system, initially, the MR is arbitrarily kept constant as 50 and the experiments were conducted for FR 40, 50, and 60. Similarly, to find the best possible MR, the FR is taken as 50 and then the experiments were conducted for MR 40, 50, and 60.

2.4 Uncertainty analysis

Thermal resistance plays a major role in the heat transfer performance of a closed-loop pulsating heat pipe. For this experiment, thermal resistance is calculated as the ratio of differences in the evaporator and ambient temperatures (T_e & T_∞) to the applied heat input (Q). Heat input is found out by multiplying voltage (V) and current (I).

$$Q = V \times I \tag{2}$$

$$R = \frac{\left(T_e - T_\infty\right)}{Q} \tag{3}$$

There exists a certain uncertainty in the measurement of temperatures by thermocouples and the measurement of voltage and current using voltmeter and ammeter. Therefore, to assess the confidence in the obtained results, an uncertainty analysis is carried out.

Taking dV and dI as the uncertainties in voltage and current readings, the standard uncertainties can be given as:

$$\frac{\delta Q}{Q} = \sqrt{\left(\frac{dV}{V}\right)^2 + \left(\frac{dI}{I}\right)^2} \tag{4}$$

$$\frac{\delta R}{R} = \sqrt{\left(\frac{\delta T_e}{T_e - T_\infty}\right)^2 + \left(\frac{\delta T_\infty}{T_e - T_\infty}\right)^2 + \left(\frac{\delta Q}{Q}\right)^2} \tag{5}$$

The data logger used (Agilent 34970A) has an accuracy of ± 0.0256 °C and the calibrated J-type thermocouples have an accuracy of ± 0.1 °C. Voltage and current were measured in the range of 0–80 V and 0–3 A respectively and have an accuracy of 0.5%. For a heat input of 27 W (1 A and 27 V), $(T_e - T_\infty)$ of water–acetone at mixing ratio 50% and filling ratio 50% was found to be 13.74 °C. Therefore, the standard uncertainties are:

$$\frac{\delta Q}{Q} = \sqrt{\left(\frac{0.5\% \times 80}{27}\right)^2 + \left(\frac{0.5\% \times 3}{1}\right)^2} = 2.1\%$$

$$\frac{\delta R}{R} = \sqrt{2 \times \left(\frac{0.1 + 0.0256}{13.74}\right)^2 + (0.021)^2} = 2.46\%$$

Considering uncertainty of 2 standard deviations and approximately a 95% confidence level, coverage factor (k) is given as 2. Therefore, the expected maximum uncertainty (U_{max}) under the aforementioned conditions is:

$$U_{max} = \frac{\delta R}{R} \times K \tag{6}$$

$$U_{max} = 2.46\% \times 2 = 4.92\%$$

Similarly, uncertainties for other heat inputs (109 W and 240 W) at different working fluid ratios were calculated and found 4.92% as the maximum uncertainty observed.

3 Results and discussions

Taking water–acetone as the working fluid, experiments were carried out in still air at room temperature (25–30 °C) with different filling ratios and mixing ratios for three different heat loads of 27 W, 109 W, and 240 W. For each test run, more than 10 min of additional heating has been provided to ensure that the steady-state is achieved.

3.1 Temperature variation along the heating surface

Figure 5 delineates the temperature profile along the surface of the cylinder at different test runs. Since the cylinder surface represents the stator coil of the electric motor and it comparatively gives the heat dissipation occurring in the windings during the real-time operation in a motor, it is important to check the uniformity of heat distribution over the surface which is in contact with the four evaporator sections of CLPHPs (positioned 10° apart from the centre of the cylinder). In the interest of clarity, a graph showing variations on surface temperature profile along axial distance was plotted and it reveals that the average surface temperature

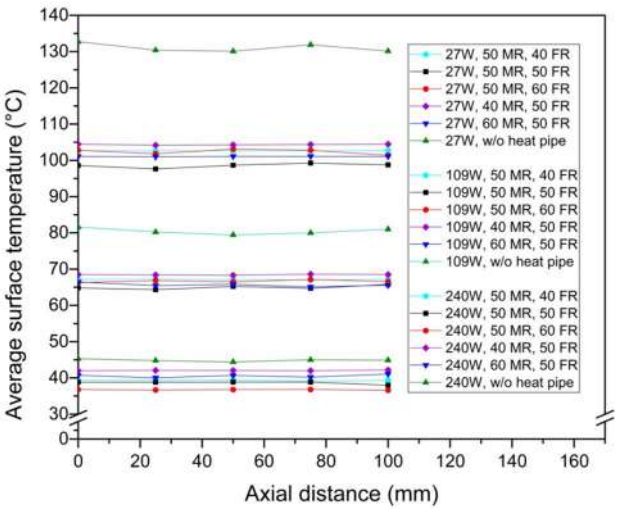

Fig. 5 Temperature profile along the axial distance

variation recorded during each test runs (represented in the legends) ensure uniform heat flux to the individual CLPHP. In addition to that, it is clear that the surface of the cylinder predominantly shows a uniform heat distribution at lower heat fluxes on all combinations of the working fluid, but very little variations were exhibited at higher heat loads which were due to the fluctuation in voltage applied since the heat load is a quadratic function of the voltage.

3.2 Temperature variation with time for different heat loads

This section discusses the differences in temperature vs. time characteristics of the motor surface with and without employing the thermal management system. Figure 6 shows temperature vs. time curves for different test combinations under each heat load 27 W, 109 W, and 240 W till the steady-state is achieved. The observed steady-state temperature and the corresponding time for each combination of working fluids are listed in Table 2.

As expected, observations made on without providing CLPHPs shows the highest steady-state temperature at a faster rate for every heat load applied. From Fig. 6a it is clear that by keeping MR constant at 50%, the lowest steady-state temperature (36.9 °C) is achieved by the working fluid taken at 60 FR in 82 min. But at the same time the working fluid taken at 50 FR reached a steady state at 38.74 °C in 100 min. The steady-state temperature difference between 60 FR and 50 FR is 1.84 °C while the time required to reach steady state is about 100 min. This shows that 50 FR-50 MR combination at lower heat input has prolonged heat management as a result of the higher rate of heat transfer from the cooling pads to the condenser section by initiating the liquid–vapour slug flow. When FR was kept constant at 50%, the lowest

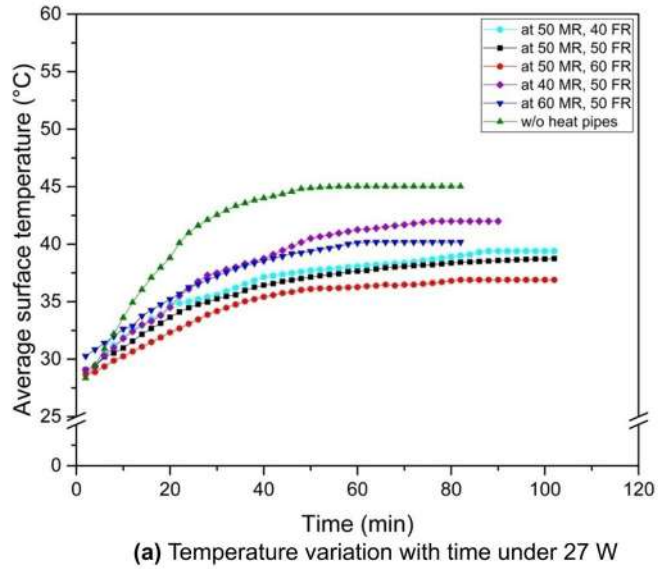

(a) Temperature variation with time under 27 W

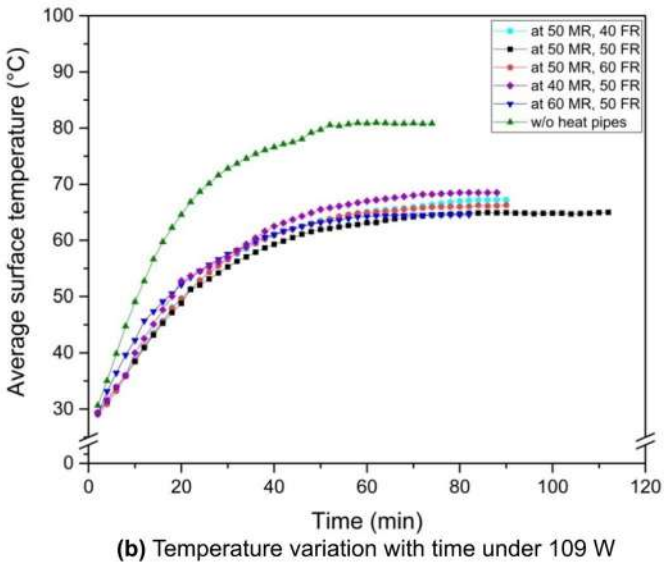

(b) Temperature variation with time under 109 W

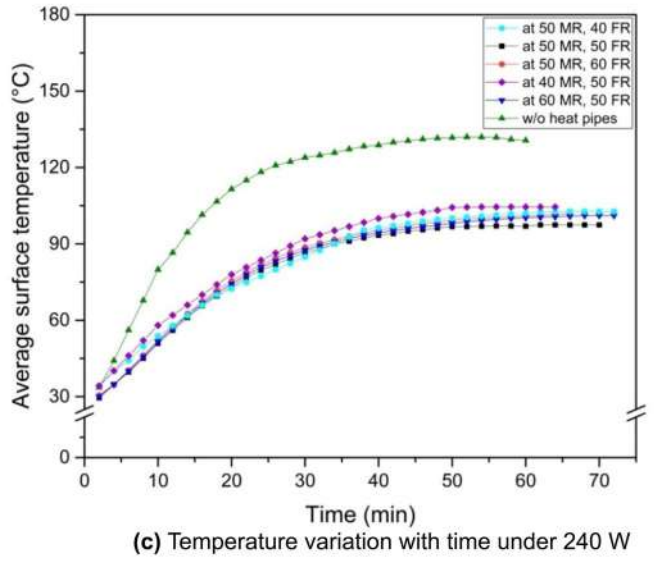

(c) Temperature variation with time under 240 W

Fig. 6 **(a)** Temperature variation with time under 27 W **(b)** Temperature variation with time under 109 W **(c)** Temperature variation with time under 240 W. Average surface temperature variation of the cooling pad to reach the steady-state condition under different heat loads

Table 2 Average Surface Temperature of cooling pad for a heat load of 27 W

SL.No	Combination	Average Surface Temperature(°C)	Time to attain Steady State (min.)
1	40 FR – 50 MR	39.40	88
2	50 FR – 50 MR	38.74	100
3	60 FR – 50 MR	36.90	82
4	50 FR – 40 MR	42.00	76
5	50 FR – 60 MR	40.18	62
6	Without Cooling System	45.02	58

steady-state temperature is shown by the working fluid taken at 50% MR. Meanwhile, 50 FR-40 MR mixture attains the highest temperature. This is due to the higher fraction of water content in this particular combination which initially resists the pulsating action at lower heat load because water has a higher boiling point, surface tension and overall higher start-up heat input than that of acetone [12].

When the heat load is increased to 109 W, observations from Fig. 6b and the corresponding readings from Table 3, indicate similar conditions as explained in the 27 W heat load. I.e. among the lowest consecutive steady-state temperatures, 50 FR-50 MR shows better heat transfer characteristics than 50 FR-60 MR combination. Also, Fig. 6b shows the onset of dry-out condition at 40 FR- 50 MR, since the temperature curve begins to rise at 38 min after starting.

On increasing the heat load to 240 W (Fig. 6c), the rate at which temperature increases becomes faster and reaches steady-state within a short period compared to lower heat loads (Table 4). At 240 W without the cooling system, the surface temperature rises to 130.65 °C. Meanwhile, the thermal management system with 50 FR-50 MR managed to cool down the motor surface by 33.3 °C. The progressive dry-out condition is exhibited by the curves 40 MR-50 FR and 50 MR-40 FR since the rate of change of temperature is higher.

Table 3 Average Surface Temperature of cooling pad for a heat load of 109 W

SL.No	Combination	Average Surface Temperature (°C)	Time to attain Steady State (min.)
1	40 FR – 50 MR	67.20	84
2	50 FR – 50 MR	64.99	112
3	60 FR – 50 MR	66.27	90
4	50 FR – 40 MR	68.50	80
5	50 FR – 60 MR	64.56	76
6	Without Cooling System	80.82	74

Table 4 Average Surface Temperature of cooling pad for a heat load of 240 W

SL.No	Combination	Average Surface Temperature (°C)	Time to attain Steady State (min.)
1	40 FR – 50 MR	102.70	66
2	50 FR – 50 MR	97.440	62
3	60 FR – 50 MR	101.86	66
4	50 FR – 40 MR	104.50	54
5	50 FR – 60 MR	101.12	68
6	Without Cooling System	130.65	60

3.3 Effect on variation of overall heat transfer coefficient with heat flux

In order to understand the thermal performance of the CLPHP system, the overall heat transfer coefficients for different working conditions under varying heat loads are compared and discussed. The overall heat transfer coefficient is calculated using the formula,

$$U = \frac{Q}{A\Delta T} \tag{7}$$

where Q is the total heat supplied (W), A is the curved surface area of the motor/heat-generating surface in direct contact with cooling pads (m^2) and ΔT (K) is the difference in temperatures between evaporator (steady-state) and ambient condition.

From Fig. 7, it is evident that for lower heat fluxes, 50 MR-60 FR working fluid shows the highest overall heat transfer coefficient followed by the 50 MR-50 FR combination as 56.11 W/m^2K and 49.58 W/m^2K respectively.

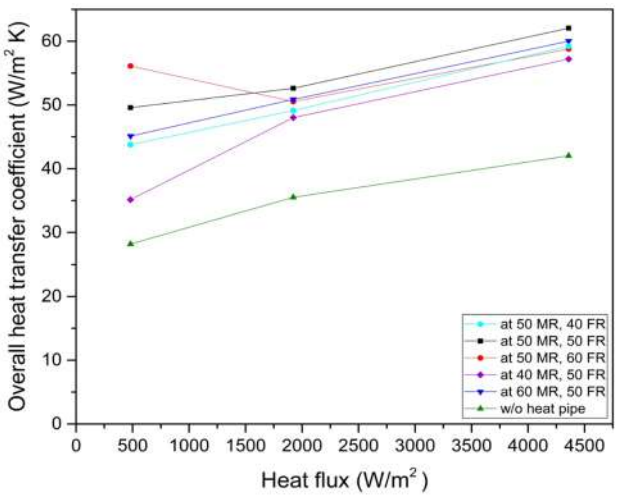

Fig. 7 Overall heat transfer coefficients vs. Heat flux

Among all the working fluid conditions tested, 40 MR-50 FR displays the lowest heat transfer coefficient because the mixing ratio has a higher percentage of water content which causes an increase in effective surface tension of the fluid. This results in slower startup and pulsating impulse. Meanwhile, under the same heat fluxes both 60 MR-50 FR and 50 MR-40 FR combinations display almost similar characteristics. Therefore it is clear from this study that variation in MR makes a wide difference in the thermal characteristics at lower heat fluxes than variations in FR.

As the heat flux increases to 2000 W/m^2 thermal characteristics were observed as close to each other, also pulsating fluid regime tends to take a fixed direction and amplitude of slug oscillation increases with increase in heat flux and become comparable with system length [23]. But the 50 MR-50 FR case presents the better thermal characteristics among all other working fluid combinations. It has to be noted that, without the cooling system, the motor surface attains an overall heat transfer coefficient of 35.8 W/m^{2}K. I.e. almost 47% of the increase in overall heat transfer coefficients is achieved by 50 MR-50 FR under this heat flux. On further increasing the heat flux to 4300 W/m^2, irrespective of the mixing ratio, overall heat transfer improved to a good extent for every combination. But, still 50 MR-50 FR shows higher heat transfer rate with overall heat transfer coefficients of 62.1 W/m^{2}K, indicating effective re-circulation of liquid–vapour slugs within the four CLPHPs at higher heat fluxes. On examining the thermal behaviour of overall heat transfer coefficient under each working conditions, water–acetone mixture with 50 MR-50 FR exhibits better heat transfer characteristics in all ranges of heat fluxes than 50 MR- 60 FR combination.

4 Effect of variation on thermal resistance with heat flux

The thermal resistance of CLPHP system at different operating conditions is shown in Fig. 8. The thermal resistance (R) is determined by applying the formula

$$R = \frac{\left(T_e - T_\infty\right)}{Q} \tag{8}$$

where, $\left(T_e - T_\infty\right)$ is the difference between evaporator and ambient temperatures, Q is the heat load at which the experiments are carried out.

The closed-loop pulsating heat pipes were employed in a way that the evaporator section with cooling pads almost encases the heating surface. As a result, it reduces the overall thermal resistance compared to natural convection. From the graph it is clear that the behaviour of CLPHP for different FR and MR under lowest heat flux were distinct. 40 MR-50 FR shows the highest thermal resistance at lower heat flux. This is because of the insufficient generation of impetus due to a higher fraction of water content and makes the system incapable of generating adequate perturbations which results drop in bubble pumping effect at lower heat flux. However, 50 MR-60 FR exhibits the lowest thermal resistance under this heat flux. The thermal resistance of CLPHP under all cases drops down as the heat flux increases to 2000 W/m^2 except 50 MR-60 FR, which shows an increase in thermal resistance at lower heat flux. This is because at lower heat inputs the phase change of working fluid with high FR occurs relatively slower than that in higher heat input. Additionally, on increasing the filling ratio, a large percentage of the volume of CLPHP is filled with the working fluid and as a result formation of bubble slugs will be space-constrained. Therefore, water–acetone fails to reach adequate flow velocity, leading to a decrease in the ability to transfer heat energy and thus thermal resistance increases. When the heat flux is further increased to 4300 W/m^2, 50 FR-50 MR again drops to 0.29 K/W, which is the lowest thermal resistance attained under this condition.

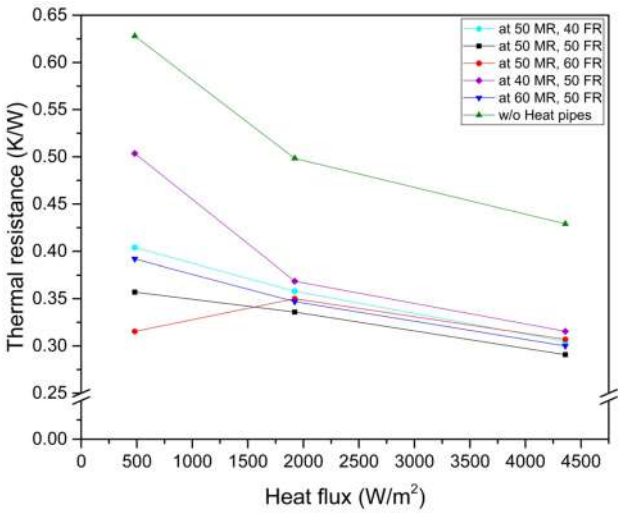

Fig. 8 Thermal resistance vs. Heat flux

On evaluating the results obtained from the graphs, we can conclude that 50 MR-50 FR has better thermal characteristics with the lowest thermal resistance as the heat flux increases within the scope of this study.

5 Conclusions

The experimental investigation of a closed-loop pulsating heat pipe-based cooling system for electric motor thermal management has been conducted successfully. The cooling system was tested for various mixing ratio and filling ratio combinations of the water–acetone binary fluids in three

different heat inputs (27 W, 109 W and 240 W) and the following major conclusions were procured from the results:

- The curved planar CLPHP used in this work was found to be working successfully in horizontally oriented testing. The maximum operating temperature of the CLPHP arrangement was limited to 130 °C for effective heat transfer to occur in the water–acetone binary mixture without undergoing dry-out conditions.
- On evaluating the thermal characteristics of the system under different working conditions, 50 MR-50 FR was found to be the optimum working condition for this system as it exhibits the lowest thermal resistance on increasing the heat flux. Also, the distinct behaviour of water–acetone in different mixing ratios and filling ratios were studied. On lower heat loads and higher filling ratios (FR > 50%), the working fluid has relatively high thermal resistance because the water–acetone mixture will be occupying the majority of the CLPHP volume and thus the formation of bubble slugs within the heat pipes will be space-constrained, This results in a drop in flow velocity of the binary fluid within the heat pipe arrangement, leading to inefficient heat transfer between evaporator and condenser sections.
- The optimum working conditions for this CLPHP cooling system was found to be the water–acetone mixture at 50 MR-50 FR working at a temperature below 130 °C. The designed cooling system working in conjunction with the natural convection of the motor surface was able to reduce the thermal resistance from 0.42 K/W to 0.29 K/W at a heat supply of 240 W. I.e., a 31% reduction in thermal resistance and an increase in the overall heat transfer rate by 47% passively.

Acknowledgements The authors of this work would like to thank the authorities of "Sree Chitra Thirunal College of Engineering", Trivandrum for their support to complete the experiment successfully. Also, the authors would like to acknowledge the authorities of "Brahmos Aerospace Trivandrum Ltd" for their technical support during the experimentation.

Funding No funding was received for conducting this study.

Data availability The datasets generated during and/or analysed during the current study are available from the corresponding author on reasonable request.

Code availability Not applicable.

Declarations

Conflict of interests All authors have no conflict of interest to report.

Financial/non-financial interests The authors have no relevant financial or non-financial interests to disclose.

References

1. Bonnett AH (2000) Operating temperature considerations and performance characteristics for IEEE 841 motors. In Record of Conference Papers. Industry Applications Society Forty-Seventh Annual Conference. 2000 Petroleum and Chemical Industry Technical Conference (Cat. No. 00CH37112). IEEE . 77–89. https://doi.org/10.1109/PCICON.2000.882764
2. Cassat A, Espanet C, Wavre N (2003) BLDC motor stator and rotor iron losses and thermal behavior based on lumped schemes and 3-D FEM analysis. IEEE Trans Ind Appl 39(5):1314–1322. https://doi.org/10.1109/TIA.2003.816480
3. Moosavi SS, Djerdir A, Amirat YA, Khaburi DA (2015) Demagnetization fault diagnosis in permanent magnet synchronous motors: A review of the state-of-the-art. J Magn Magn Mater 391:203–212. https://doi.org/10.1016/j.jmmm.2015.04.062
4. Fakhfakh MA, Kasem MH, Tounsi S, Neji R (2008) Thermal analysis of a permanent magnet synchronous motor for electric vehicles. Journal of Asian Electric Vehicles 6(2):1145–1151. https://doi.org/10.4130/jaev.6.1145
5. Dunn PD, Reay DA (1973) The heat pipe. Phys Technol 4(3):187. https://doi.org/10.1088/0305-4624/4/3/I01
6. Almahmoud S, Jouhara H (2019) Experimental and theoretical investigation on a radiative flat heat pipe heat exchanger. Energy 174:972–984. https://doi.org/10.1016/j.energy.2019.03.027
7. Groll M, Krahling H, Munzel WD (1978) Heat pipes for cooling of an electric motor. Journal of Energy 2(6):363–367. https://doi.org/10.2514/3.62387
8. Putra N, Ariantara B (2017) Electric motor thermal management system using L-shaped flat heat pipes. Appl Therm Eng 126:1156–1163. https://doi.org/10.1016/j.applthermaleng.2017.01.090
9. Akachi H (1996) Pulsating heat pipes. In Proceedings 5th International Heat Pipe Symp., 1996
10. Khandekar S, Groll M, Charoensawan P, Rittidech S, Terdtoon P (2004) Closed and open loop pulsating heat pipes. In K-4, Proceedings of 13th International Heat Pipe Conference. China Academy of Space Technology Shanghai, China
11. Yang H, Khandekar S, Groll M (2008) Operational limit of closed loop pulsating heat pipes. Appl Therm Eng 28(1):49–59. https://doi.org/10.1016/j.applthermaleng.2007.01.033
12. Patel VM, Mehta HB (2017) Influence of working fluids on startup mechanism and thermal performance of a closed loop pulsating heat pipe. Appl Therm Eng 110:1568–1577. https://doi.org/10.1016/j.applthermaleng.2016.09.017
13. Mozumder AK, Akon AF, Chowdhury MSH, Banik SC (2010) Performance of heat pipe for different working fluids and fill ratios. Journal of Mechanical Engineering 41(2):96–102. https://doi.org/10.3329/jme.v41i2.7473
14. Wilson C, Borgmeyer B, Winholtz RA, Ma HB, Jacobson D, Hussey D (2011) Thermal and visual observation of water and acetone oscillating heat pipes. J Heat Transf 133(6). https://doi.org/10.1115/1.4003546
15. Zhu Y, Cui X, Han H, Sun S (2014) The study on the difference of the start-up and heat-transfer performance of the pulsating heat pipe with water− acetone mixtures. Int J Heat Mass Transf 77:834–842. https://doi.org/10.1016/j.ijheatmasstransfer.2014.05.042
16. Groll M, Khandekar S (2003) Pulsating heat pipes: progress and prospects. In Proc Int Conf on Energy and the Environment 1:723–730
17. Khandekar S, Dollinger N, Groll M (2003) Understanding operational regimes of closed loop pulsating heat pipes: an experimental study. Appl Therm Eng 23(6):707–719. https://doi.org/10.1016/S1359-4311(02)00237-5

18. Jang JH, Chiu HC, Yan WM, Tsai MC, Wang PY (2015) Numerical study on electromagnetics and thermal cooling of a switched reluctance motor. Case Studies in Thermal Engineering 6:16–27. https://doi.org/10.1016/j.csite.2015.05.001
19. Pyrhönen J, Lindh P, Polikarpova M, Kurvinen E, Naumanen V (2015) Heat-transfer improvements in an axial-flux permanent-magnet synchronous machine. Appl Therm Eng 76:245–251. https://doi.org/10.1016/j.applthermaleng.2014.11.003
20. Park MH, Kim SC (2019) Thermal characteristics and effects of oil spray cooling on in-wheel motors in electric vehicles. Appl Therm Eng 152:582–593. https://doi.org/10.1016/j.applthermaleng.2019.02.119
21. Semidey SA, Mayor JR (2014) Experimentation of an electric machine technology demonstrator incorporating direct winding heat exchangers. IEEE Trans Industr Electron 61(10):5771–5778. https://doi.org/10.1109/TIE.2014.2303779
22. Wang R, Wang Y, Feng C, Zhang X (2015) Powertrain preheating system of tracked hybrid electric vehicle in cold weather. Appl Therm Eng 91:252–258. https://doi.org/10.1016/j.applthermaleng.2015.08.027
23. Khandekar S, Groll M (2003) On the definition of pulsating heat pipes: an overview. In Proc 5th Minsk Int Conf (Heat Pipes, Heat Pumps and Refrigerators), Minsk, Belarus 707–719